nature physics

LETTERS

https://doi.org/10.1038/s41567-020-0965-y

Check for updates

Chiral phonons in the pseudogap phase of cuprates

G. Grissonnanche[1]✉, S. Thériault[1], A. Gourgout[1], M.-E. Boulanger[1], E. Lefrançois[1], A. Ataei[1], F. Laliberté[1], M. Dion[1], J.-S. Zhou[2], S. Pyon[3,4], T. Takayama[3,5], H. Takagi[3,5,6,7], N. Doiron-Leyraud[1] and L. Taillefer[1,8]✉

The nature of the pseudogap phase of cuprates remains a major puzzle[1,2]. One of its signatures is a large negative thermal Hall conductivity[3], whose origin is as yet unknown. This is observed even in the undoped Mott insulator La_2CuO_4, in which the charge carriers are localized and therefore cannot be responsible. Here, we show that the thermal Hall conductivity of La_2CuO_4 is roughly isotropic; that is, for heat transport parallel and normal to the CuO_2 planes, it is nearly the same. This shows that the Hall response must come from phonons, as they are the only heat carriers that are able to move with the same ease both normal and parallel to the planes[4]. For doping levels higher than the critical doping level at which the pseudogap phase ends, both $La_{1.6-x}Nd_{0.4}Sr_xCuO_4$ and $La_{1.8-x}Eu_{0.2}Sr_xCuO_4$ show no thermal Hall signal for a heat current normal to the planes, which establishes that phonons have zero Hall response outside the pseudogap phase. Inside the pseudogap phase, the phonons must become chiral to generate the Hall response, but the mechanism by which this happens remains to be identified. It must be intrinsic (from a coupling of phonons to their electronic environment) rather than extrinsic (from structural defects or impurities), as these are the same on both sides of critical doping.

The thermal Hall effect has emerged as a fruitful probe of insulators[5–7], which are materials in which the electrical Hall effect is zero because there are no mobile charge carriers. In the presence of a heat current J along the x axis and a magnetic field H along the z axis, a transverse temperature gradient ∇T (along the y axis) can develop even if the carriers of heat are neutral (chargeless), provided that they have chirality[8]. In particular, carriers with a Berry curvature, whether they are fermions or bosons, in general will generate a non-zero thermal Hall conductivity, κ_{xy} (refs. [9,10]). So, a measurement of the thermal Hall effect can potentially reveal various topological excitations in quantum materials; for example, Majorana edge modes in chiral spin liquids[11–13].

However, phonons can in fact also generate a non-zero thermal Hall conductivity if some mechanism, either intrinsic[9] or extrinsic[14], confers chirality to the phonons. (Here, we use the term 'chirality' to mean handedness in the presence of a magnetic field.) The phonon κ_{xy} signal can be large, as is the case for multiferroic materials[15] and for strontium titanate ($SrTiO_3$; ref. [16]). In multiferroic materials, the signal is caused by spin-phonon coupling, whereas in $SrTiO_3$, the cause appears to involve structural domain boundaries.

In cuprates, a large negative κ_{xy} signal was observed at a low temperature inside the pseudogap phase, for doping levels $p < p^\star$ (ref. [3]). As this negative κ_{xy} persists at levels as low as $p = 0$ in the Mott insulator state, it cannot come from charge carriers. Therefore, it must come from either spin-related excitations (which are possibly topological[17,18]) or phonons[19]. To distinguish between these two types of heat carrier, we adopt a simple approach: we measure the thermal Hall conductivity for a heat current along the c axis, normal to the CuO_2 planes, a direction in which only phonons move easily[4] (see Methods).

First, we look at the undoped cuprate La_2CuO_4, a Mott insulator with no mobile charge carriers. Here, phonons are the dominant heat carriers at low temperatures, and their longitudinal thermal conductivity $\kappa_{nn}(T)$ is nearly the same for $J \parallel a$ ($n = x$) and $J \parallel c$ ($n = z$) (ref. [4]; see Methods). As shown in Fig. 1a, the in-plane thermal Hall conductivity κ_{xy} of La_2CuO_4 ($J \parallel -x \perp c$, $H \parallel z$ and $\nabla T \parallel y$; Extended Data Fig. 1a) was found previously to be negative at all T, with $|\kappa_{xy} / T|$ growing steadily as temperature is decreased below 100 K, reaching one of the largest Hall conductivities of any insulator at $T = 10$ K (ref. [3]). In a separate sample of La_2CuO_4, we measured κ_{zy} ($J \parallel z \parallel c$, $H \parallel x$ and $\nabla T \parallel y$; Extended Data Fig. 1b) and found that $\kappa_{zy}(T) \approx \kappa_{xy}(T)$ for all T (Fig. 1a). The fact that the thermal Hall conductivity is as large across the CuO_2 planes as it is along the planes is strong evidence that the carriers of heat responsible for the thermal Hall effect in La_2CuO_4 are phonons. Indeed, any excitation of electronic origin (that carries charge or spin) is expected to be much more mobile along the CuO_2 planes as opposed to across planes (see Methods).

Next, we examine the hole-doped cuprate $La_{1.6-x}Nd_{0.4}Sr_xCuO_4$ (Nd-LSCO; see phase diagram in Fig. 2a). The pseudogap phase boundary $T^\star(p)$ ends at a $T = 0$ critical point $p^\star = 0.23$, as determined by both transport[20] and photoemission (ARPES; ref. [21]) measurements. At $p = 0.24$, just above $p^\star$, the in-plane thermal Hall conductivity κ_{xy} of Nd-LSCO was found to be positive at all T (Fig. 1b) and in good agreement with the Wiedemann–Franz law, which states $\kappa_{xy} / T = L_0 \sigma_{xy}$ as $T \to 0$ K, where $L_0 = (\pi^2/3)(k_B / e)^2$ (ref. [3]). Using a sample cut from the same large crystal, we measured κ_{zy} and found that $\kappa_{zy}(T) = 0$ at all T, below 100 K (Fig. 1b). Not only is the Wiedemann–Franz law satisfied for $J \parallel a$, our data for $J \parallel c$ show

[1]Département de physique, Institut quantique, and RQMP, Université de Sherbrooke, Sherbrooke, Québec, Canada. [2]Materials Science and Engineering Program, Department of Mechanical Engineering, University of Texas at Austin, Austin, TX, USA. [3]Department of Advanced Materials Science, University of Tokyo, Kashiwa, Japan. [4]Department of Applied Physics, University of Tokyo, Tokyo, Japan. [5]Max Planck Institute for Solid State Research, Stuttgart, Germany. [6]Department of Physics, University of Tokyo, Tokyo, Japan. [7]Institute for Functional Matter and Quantum Technologies, University of Stuttgart, Stuttgart, Germany. [8]Canadian Institute for Advanced Research, Toronto, Ontario, Canada. ✉e-mail: gael.grissonnanche@usherbrooke.ca; louis.taillefer@usherbrooke.ca

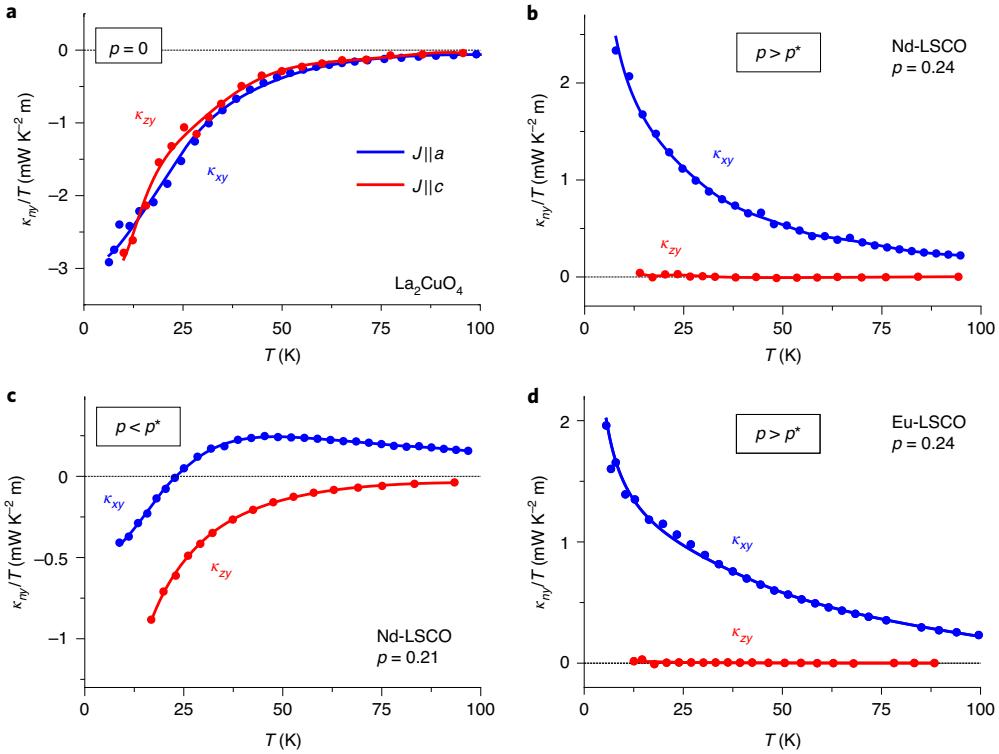

Fig. 1 | Thermal Hall conductivity of cuprates at three different dopings. a–d, Thermal Hall conductivity versus temperature in a field of magnitude $H = 15$ T, plotted as κ_{ny} / T versus T for two heat current directions, $J \parallel a$ ($n = x$; blue) and $J \parallel c$ ($n = z$; red), in La_2CuO_4 ($p = 0$) (**a**), $La_{1.6-x}Nd_{0.4}Sr_xCuO_4$ (Nd-LSCO) with $p = 0.24$ (**b**), Nd-LSCO with $p = 0.21$ (**c**) and $La_{1.8-x}Eu_{0.2}Sr_xCuO_4$ with $p = 0.24$ (**d**). All lines are guides to the eye. The κ_{xy} data are from ref. [3]; in Nd-LSCO, they were taken in a field with $H = 18$ T and so are multiplied by a factor of 15/18 here.

that phonons in Nd-LSCO have no Hall effect at $p = 0.24$ for any direction of motion. (Note that the contribution of charge carriers to $\kappa_{zy}(T)$ is extremely small; see Methods.) In other words, phonons have no chirality outside of the pseudogap phase.

In the related material $La_{1.8-x}Eu_{0.2}Sr_xCuO_4$ (Eu-LSCO), which also has $p^\star = 0.23$ (ref. [22]), we find again that $\kappa_{zy}(T) = 0$ at $p = 0.24 > p^\star$ (Fig. 1d). The fact that $\kappa_{zy}(T) = 0$ down to 10 K (on two separate samples) shows that our measurement technique does not introduce any spurious background Hall signal (see Methods). That is, any thermal Hall signal coming from the sample mount is negligible compared to the signal from the samples.

Inside the pseudogap phase ($p < p^\star$), a large negative κ_{xy} was observed at low T in $La_{2-x}Sr_xCuO_4$ (LSCO) with $p = 0.06$, Eu-LSCO with $p = 0.08$, $Bi_2Sr_{2-x}La_xCuO_{6+\delta}$ with $x = 0.2$ and Nd-LSCO with $p = 0.20$, 0.21 and 0.22 (ref. [3]). In Fig. 1c, we show the published κ_{xy} data for Nd-LSCO with $p = 0.21$, which become negative below 25 K. This is in contrast to σ_{xy}, which remains positive as $T \to 0$ (refs. [3,20]). In the same figure, we report our data for κ_{zy} as measured in Nd-LSCO with $p = 0.21$. We see that there is now a sizeable (negative) κ_{zy} signal, in contrast to that at $p = 0.24$.

We summarize our κ_{zy} measurements in Fig. 2b. At $p = 0.24$, just outside the pseudogap phase ($p > p^\star$; Fig. 2a), $\kappa_{zy}(T) = 0$ and phonons have no chirality. At $p = 0.21$, just inside the pseudogap phase ($p < p^\star$; Fig. 2a), $\kappa_{zy}(T) \ll 0$ and phonons have suddenly acquired chirality. This new phonon Hall effect is of comparable magnitude throughout the pseudogap phase, from $p^\star$ down to $p = 0$, when measured relative to κ_{nn} ($|\kappa_{ny} / \kappa_{nn}| \approx 0.3$–$0.5$ at $H = 15$ T and $T = 20$ K). Therefore, we have two key findings: the large negative thermal Hall signal in cuprates is carried by phonons, and the phonons become chiral only once they enter the pseudogap phase. (In ref. [3], a phonon scenario was considered unlikely because of the small size of two expected signatures, a field dependence of κ_{xx} and a drop in κ_{xx} below $p^\star$; see Methods.)

The question then becomes what special property of the pseudogap phase confers chirality to phonons. One possibility is that phonons acquire Berry curvature[9] from their interaction with the special electronic properties of that phase. A rather universal consequence of Berry curvature is the production of a thermal Hall response that varies as $\kappa_{xy} / T \propto \exp(-T/T_0)$ at intermediate temperatures[10]. In Fig. 3, we show a fit of our κ_{zy} data to the relation $\kappa_{zy} / T = A \exp(-T/T_0) + C$, for La_2CuO_4 and Nd-LSCO with $p = 0.21$. We see that the fits are excellent, down to $T \approx T_0 \approx 15$ K. This supports the scenario in which phonons have Berry curvature below $p^\star$.

Further experimental and theoretical work is needed to identify the microscopic mechanism responsible for the chirality of phonons in the pseudogap phase. Note that it cannot simply be the skew scattering of phonons from impurities. Indeed, although skew scattering of phonons by rare-earth impurities can produce a thermal Hall effect[14,23], this extrinsic impurity-related mechanism cannot apply here, as for the same Nd-LSCO material (with the same impurities) we find zero thermal Hall effect when $p > p^\star$. Also, changing non-magnetic Eu ions for magnetic Nd ions in $La_{2-y-x}RE_ySr_xCuO_4$ (RE = Eu,Nd), at $p = 0.24$, still yields zero phonon Hall signal. What is needed is a qualitative change below $p^\star$ in the intrinsic coupling of phonons to their environment. A recent ARPES study[24] in the cuprate $Bi_2Sr_2CaCu_2O_{8+\delta}$ saw a rapid increase in the coupling of phonons to electrons upon crossing below $p^\star$.

A large κ_{xy} signal due to phonons was recently observed in $SrTiO_3$, but not in the related material $KTaO_3$, for which $\kappa_{xy}(T) \approx 0$ below 100 K (ref. [16]). This difference was attributed to the presence of structural domains in $SrTiO_3$ that are absent in $KTaO_3$. Exactly how structural domains can generate a Hall effect is still unclear[19],

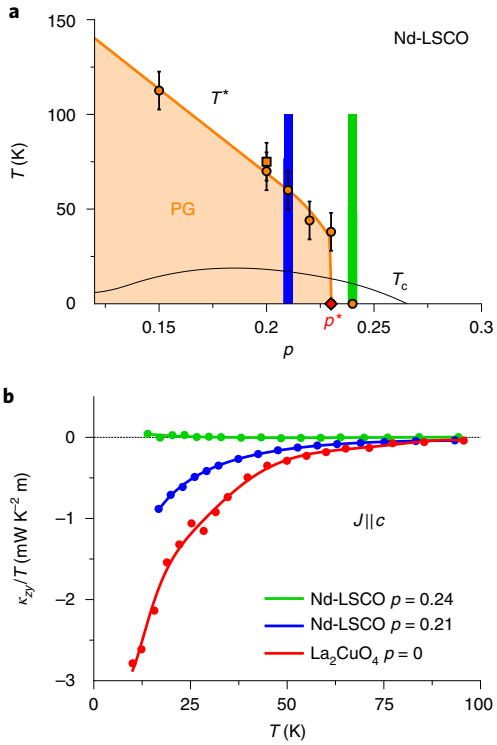

Fig. 2 | Evolution of the *c*-axis thermal Hall conductivity across the phase diagram. a, Temperature–doping phase diagram of Nd-LSCO, showing the superconducting transition temperature T_c (black line; zero field) and the pseudogap phase below T^* (PG; orange region), which ends at the critical doping $p^* = 0.23$ (diamond) for both Nd-LSCO[2,20] and $La_{1.8-x}Eu_{0.2}Sr_xCuO_4$ (ref. [22]). The orange circles indicate the temperature below which the in-plane resistivity deviates upwards from its linear T dependence at high temperature (refs. [20,33]; the error bars, taken from ref. [20], reflect the uncertainty in pinpointing the start of that gradual upturn). The orange square marks the onset temperature for the opening of the anti-nodal pseudogap in Nd-LSCO at $p = 0.20$ as detected by ARPES (ref. [21]); the error bar is given by the temperature spacing of the ARPES data. The two vertical bands indicate the two dopings on either side of p^* at which we measured $\kappa_{zy}(T)$, the *c*-axis thermal Hall conductivity shown in part **b** (blue for $p = 0.21$, green for $p = 0.24$). **b**, Thermal Hall conductivity κ_{zy}, for a heat current normal to the CuO_2 planes ($J \parallel c \parallel z$) and a magnetic field of 15 T applied parallel to the planes ($H \parallel a \parallel x$), plotted as κ_{zy} / T versus T, in La_2CuO_4 ($p = 0$; red), Nd-LSCO with $p = 0.21$ (blue) and Nd-LSCO with $p = 0.24$ (green).

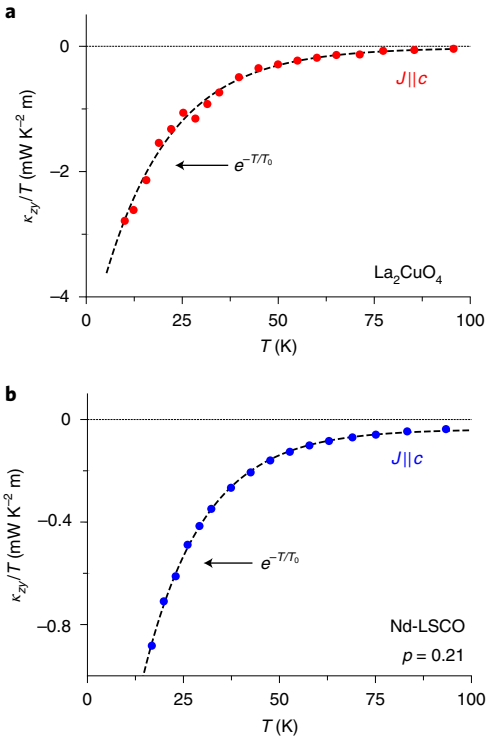

Fig. 3 | Phenomenological fit to the phonon thermal Hall conductivity. a,**b**, Fit of the thermal Hall conductivity $\kappa_{zy}(T)$ in La_2CuO_4 (**a**) and Nd-LSCO at $p = 0.21$ (**b**) to the phenomenological expression $\kappa_{zy} / T = A \exp(-T/T_0) + C$, derived from a theory that links the thermal Hall effect to the Berry curvature of the heat carriers[10]. The fit interval is from 15 K to 100 K. The resulting fit parameters are $A = -4.9$ mW K^{-2} m, $C = -0.02$ mW K^{-2} m, $T_0 = 17.5$ K (for **a**), and $A = -2.4$ mW K^{-2} m, $C = -0.04$ mW K^{-2} m, $T_0 = 15.8$ K (for **b**). The fact that the theoretical expression fits the data well in the temperature range above T_0 supports the hypothesis that phonons in those cuprates have a non-zero Berry curvature.

but this mechanism cannot be responsible for the phonon Hall effect in Nd-LSCO. Indeed, there is no change in the crystal structure of Nd-LSCO between $p = 0.21$ and $p = 0.24$, two dopings that are both located in the so-called low-temperature tetragonal (LTT) phase (see Methods).

A large κ_{xy} signal due to phonons was observed in multiferroic materials such as $Fe_2Mo_3O_8$ (ref. [15]), in which it was attributed to a coupling of phonons to spins. A spin-phonon coupling could be relevant in the case of cuprates, given that the pseudogap phase is characterized by short-range antiferromagnetic correlations and spin singlet formation, according to numerical solutions of the Hubbard model[25]. It may be that the topological character of this unusual state of correlated spins[26] confers chirality to phonons. Note that slow antiferromagnetic correlations (quasi-static moments) are indeed observed for dopings up to p^* in Nd-LSCO[27] and LSCO[28], but not above.

The broad implication of our findings in cuprates is that phonons in insulators can generate large thermal Hall signals. All possible mechanisms for phonon chirality should be explored (for example, refs. [9,19,29,30]). Also, the possible role of phonons in causing the thermal Hall effect observed in materials such as the two-dimensional Kitaev insulator α-$RuCl_3$ (refs. [31,32]) or the frustrated magnet $Tb_2Ti_2O_7$ (refs. [7,30]) should be considered.

Online content

Any methods, additional references, Nature Research reporting summaries, source data, extended data, supplementary information, acknowledgements, peer review information; details of author contributions and competing interests; and statements of data and code availability are available at https://doi.org/10.1038/s41567-020-0965-y.

Received: 20 March 2020; Accepted: 12 June 2020;
Published online: 20 July 2020

References

1. Keimer, B. et al. From quantum matter to high-temperature superconductivity in copper oxides. *Nature* **518**, 179–186 (2015).
2. Proust, C. & Taillefer, L. The remarkable underlying ground states of cuprate superconductors. *Annu. Rev. Condens. Matter Phys.* **10**, 409–429 (2019).
3. Grissonnanche, G. et al. Giant thermal Hall conductivity in the pseudogap phase of cuprate superconductors. *Nature* **571**, 376–380 (2019).
4. Hess, C. et al. Magnon heat transport in doped La_2CuO_4. *Phys. Rev. Lett.* **90**, 197002 (2003).

5. Onose, M. et al. Observation of the magnon Hall effect. *Science* **329**, 297–299 (2010).
6. Katsura, H., Nagaosa, N. & Lee, P. A. Theory of the thermal Hall effect in quantum magnets. *Phys. Rev. Lett.* **104**, 066403 (2010).
7. Hirschberger, M. et al. Large thermal Hall conductivity of neutral spin excitations in a frustrated quantum magnet. *Science* **348**, 106–109 (2015).
8. Lee, H., Han, J. H. & Lee, P. A. Thermal Hall effect of spins in a paramagnet. *Phys. Rev. B* **91**, 125413 (2015).
9. Qin, T., Zhou, J. & Shi, J. Berry curvature and the phonon Hall effect. *Phys. Rev. B* **86**, 104305 (2012).
10. Yang, Y.-F., Zhang, G.-M. & Zhang, F.-C. Universal behavior of the anomalous thermal Hall conductivity. *Phys. Rev. Lett.* **124**, 186602 (2020).
11. Nasu, J., Yoshitake, J. & Motome, Y. Thermal transport in the Kitaev model. *Phys. Rev. Lett.* **119**, 127204 (2017).
12. Ye, M. et al. Quantization of the thermal Hall conductivity at small Hall angles. *Phys. Rev. Lett.* **121**, 147201 (2018).
13. Vinkler-Aviv, Y. & Rosch, A. Approximately quantized thermal Hall effect of chiral liquids coupled to phonons. *Phys. Rev. X* **8**, 031032 (2018).
14. Mori, M. et al. Origin of the phonon Hall effect in rare-Earth garnets. *Phys. Rev. Lett.* **113**, 265901 (2014).
15. Ideue, T. et al. Giant thermal Hall effect in multiferroics. *Nat. Mater.* **16**, 797–802 (2017).
16. Li, X. et al. Phonon thermal Hall effect in strontium titanate. *Phys. Rev. Lett.* **124**, 105901 (2020).
17. Samajdar, R. et al. Enhanced thermal Hall effect in the square-lattice Néel state. *Nat. Phys.* **15**, 1290–1294 (2019).
18. Han, J. H., Park, J.-H. & Lee, P. A. Consideration of thermal Hall effect in undoped cuprates. *Phys. Rev. B* **99**, 205157 (2019).
19. Chen, J.-Y., Kivelson, S. A. & Sun, X.-Q. Enhanced thermal Hall effect in nearly ferroelectric insulators. *Phys. Rev. Lett.* **124**, 167601 (2020).
20. Collignon, C. et al. Fermi-surface transformation across the pseudogap critical point of the cuprate superconductor $La_{2-x}Nd_{0.4}Sr_xCuO_4$. *Phys. Rev. B* **95**, 224517 (2017).
21. Matt, C. E. et al. Electron scattering, charge order and pseudogap physics in $La_{2-x}Nd_{0.4}Sr_xCuO_4$: an angle-resolved photoemission spectroscopy study. *Phys. Rev. B* **92**, 134524 (2015).
22. Michon, B. et al. Thermodynamic signatures of quantum criticality in cuprate superconductors. *Nature* **567**, 281–222 (2019).
23. Strohm, C., Rikken, G. L. J. A. & Wyder, P. Phenomenological evidence for the phonon Hall effect. *Phys. Rev. Lett.* **95**, 155901 (2005).
24. He, Y. et al. Rapid change in superconductivity and electron-phonon coupling through the critical point in Bi-2212. *Science* **362**, 62–65 (2019).
25. Kyung, B. et al. Pseudogap induced by short-range spin correlations in a doped Mott insulator. *Phys. Rev. B* **73**, 165114 (2006).
26. Scheurer, M. S. et al. Topological order in the pseudogap metal. *Proc. Natl Acad. Sci. USA* **115**, E3665–E3672 (2018).
27. Hunt, A. W. et al. Glassy slowing of stripe modulation in $(La,Eu,Nd)_{2-x}(Sr,Ba)_xCuO_4$: a ^{63}Cu and ^{139}La NQR study down to 350 mK. *Phys. Rev. B* **64**, 134525 (2001).
28. Frachet, M. *et al.* Hidden magnetism at the pseudogap critical point of a high-temperature superconductor. Preprint at https://arxiv.org/abs/1909.10258 (2019).
29. Ye, M. *et al.* Phonon dynamics in the Kitaev spin liquid. Preprint at https://arxiv.org/abs/2002.05328 (2020).
30. Hirokane, Y. et al. Phononic thermal Hall effect in diluted terbium oxides. *Phys. Rev. B* **99**, 134419 (2019).
31. Kasahara, Y. et al. Majorana quantization and half-integer thermal quantum Hall effect in a Kitaev spin liquid. *Nature* **559**, 227–231 (2018).
32. Hentrich, R. et al. Large thermal Hall effect in α-$RuCl_3$: Evidence for heat transport by Kitaev-Heisenberg paramagnons. *Phys. Rev. B* **99**, 085136 (2019).
33. Cyr-Choinière, O. et al. Pseudogap temperature T^* of cuprate superconductors from the Nernst effect. *Phys. Rev. B* **97**, 064502 (2018).

Methods

Samples. *Nd-LSCO.* Single crystals of $La_{2-y-x}Nd_ySr_xCuO_4$ (Nd-LSCO) were grown at the University of Texas at Austin, USA using a travelling-float-zone technique, with an Nd content $y=0.4$ and nominal Sr concentrations $x=0.21$ and 0.25. The hole concentration p is given by $p=x$, with an error bar $\pm$ 0.003, except for the $x=0.25$ sample, for which the doping is $p=0.24\pm0.005$ (for details, see ref. [20]). The error bars on the doping values come from the uncertainty in the Sr content x, refined with the measured values of T_c and the Hall coefficient R_H (ref. [20]).The value of T_c, defined as the point of zero resistance, is $T_c=15$ K and 11 K for samples with $p=0.21$ and 0.24, respectively. The pseudogap critical point in Nd-LSCO is at $p^*=0.23\pm0.005$ (ref. [20]). The *a*-axis ($J \parallel a$) and *c*-axis ($J \parallel c$) samples were both cut out of the same large single crystal.

Eu-LSCO. The single crystal of $La_{2-y-x}Eu_ySr_xCuO_4$ (Eu-LSCO) was grown at the University of Tokyo, Japan using a travelling-float-zone technique, with an Eu content $y=0.2$ and nominal Sr concentration $x=0.24$. The hole concentration p is given by $p=x$, with an error bar of $\pm$ 0.005. The value of T_c, defined as the point of zero resistance, is $T_c=9$ K. The pseudogap critical point in Eu-LSCO is at $p^*=0.23\pm0.005$ (ref. [22]). The *a*-axis ($J \parallel \boldsymbol{a}$) and *c*-axis ($J \parallel c$) samples were both cut out of the same large single crystal.

La_2CuO_4. Our two single crystals of La_2CuO_4 came from the same batch, grown at the University of Tokyo, Japan using a travelling-float-zone technique. The *a*-axis ($J \parallel a$) and *c*-axis ($J \parallel c$) samples were each cut out of these two single crystals, respectively.

Thermal Hall measurement. Our measurements of the *c*-axis thermal Hall conductivity κ_{zy} were performed on four samples: La_2CuO_4 ($p=0$); Nd-LSCO with $p=0.21$; Nd-LSCO with $p=0.24$; and Eu-LSCO with $p=0.24$. The in-plane thermal Hall conductivity κ_{xy} was previously reported[3] for La_2CuO_4, Nd-LSCO and Eu-LSCO at the same doping levels as used in this work. Those κ_{xy} data are shown in the four parts of Fig. 1 for comparison (blue curves).

Experimental procedure. For our measurements, six contacts are made on the sample using silver epoxy Dupont H20E diffused by annealing at high temperature in oxygen: two contacts for the heat current, two for the longitudinal temperature difference ΔT_n ($n=x$ or z) and two for the transverse temperature difference ΔT_y (Extended Data Fig. 1). The sample is glued onto a copper heat sink (Extended Data Fig. 1) with Dupont silver paint. Sample temperatures $T+$ and $T-$ are measured with one absolute type-E (chromel-constantan) thermocouple connected to $T-$ and one differential type-E thermocouple connected to $T+$ and $T-$ (which measures the temperature difference $\Delta T_n=T+-T-$). Another differential type-E thermocouple measures the transverse temperature difference ΔT_y (Extended Data Fig. 1). A finite temperature difference ΔT_n is created by applying heat to the free end of the sample (Extended Data Fig. 1), using a 5 kΩ resistor (a strain gauge from Vishay) whose resistance does not vary with temperature or field. The thermocouples and heater are connected to the sample with silver wires (25 μm and 50 μm in diameter, respectively).

The experiment is performed in a fixed magnetic field. A positive field $H=+15$ T is applied at $T=100$ K and the sample is then cooled down to $T\sim5$ K. At fixed field, the temperature is increased in steps, and the system is stabilized at each temperature point. For each point, the background voltages across all thermocouples in the absence of applied heat are carefully measured. Then heat is applied (between 0.01 mA at low temperature and 1.0 mA at high temperature) and, once the sample has reached thermal equilibrium, the thermocouple voltages are measured again. By subtracting the background voltages from the corresponding heat-on voltages, we can extract reliably the intrinsic response of the sample. We repeat this procedure at each temperature point from ~ 5 K to 100 K. Once the entire temperature range is spanned at positive field, the field is inverted at $T=100$ K to its negative value $H=-15$ T, and the system is cooled down to ~ 5 K. We then repeat the procedure under otherwise identical conditions. As always in a Hall measurement, the pure transverse signal (here ΔT_y) is obtained by anti-symmetrization: $\Delta T_y=(\Delta T_y(+15\,\mathrm{T})-\Delta T_y(-15\,\mathrm{T}))/2$.

To determine the sign of the transverse thermal Hall conductivity (the sign of ΔT_y), we use reference samples for which the sign of the thermal Hall conductivity is unambiguous: for example, overdoped $Tl_2Ba_2CuO_{6+\delta}$ (positive sign), measured using the very same set-up and thermocouple connections. For further details, see ref. [34].

For all of the κ_{zy} data reported here, the magnetic field strength is $H=15$ T. Because $H\perp c$ in this case, superconductivity is only weakly suppressed, so to report only normal-state data, we limit the data in Figs. 1–3 to $T>T_c$. For the κ_{xy} data reproduced in Fig. 1 (blue curves), the field strength was either $H=15$ T (for La_2CuO_4 and Eu-LSCO) or $H=18$ T (for Nd-LSCO; ref. [3]). In Fig. 1b,c, we have multiplied the κ_{xy} data taken at 18 T by a factor of 15/18 to enable a comparison at 15 T.

Orientation of heat current and magnetic field. In-plane heat current ($J\perp c$). For our prior measurements of κ_{xy} (ref. [3]), the heat current J was sent in the basal plane of the single crystal (along $-x$), parallel to the CuO_2 planes, generating a longitudinal temperature difference $\Delta T_x=T+-T-$ (Extended Data Fig. 1a). The longitudinal thermal conductivity along the x axis is given by $\kappa_{xx}=(J/\Delta T_x)(L_x/w_y t_z)$, where L_x is the separation (along x) between the two points at which $T+$ and $T-$ are measured, w_y is the width of the sample (along y) and t_z its thickness (along $z \parallel c$). By applying a magnetic field H along the c axis of the crystal (along z), normal to the CuO_2 planes, one generates a transverse temperature difference ΔT_y (Extended Data Fig. 1a). The in-plane thermal Hall conductivity is defined as $\kappa_{xy}=-\kappa_{yy}(\Delta T_y/\Delta T_x)(L_x/w_y)$, where κ_{yy} is the longitudinal thermal conductivity along the y axis. Here, we can take $\kappa_{yy}=\kappa_{xx}$, as all samples are either twinned or tetragonal.

Out-of-plane heat current ($J \parallel c$). For the measurements of κ_{zy} presented here, the heat current J was sent along the c axis of the single crystal (along z), perpendicular to the CuO_2 planes, generating a longitudinal temperature difference $\Delta T_z=T+-T-$ (Extended Data Fig. 1b). By applying a magnetic field H along the a axis of the crystal (along x), parallel to the CuO_2 planes, a transverse temperature difference ΔT_y is generated (Extended Data Fig. 1b). The longitudinal thermal conductivity along the z axis is given by $\kappa_{zz}=(J/\Delta T_z)(L_z/w_y t_x)$, where L_z is the separation (along z) between the two points at which $T+$ and $T-$ are measured, w_y is the width of the sample (along y) and t_x is its thickness (along $x \parallel a$). The out-of-plane thermal Hall conductivity is defined as $\kappa_{zy}=-\kappa_{yy}(\Delta T_y/\Delta T_z)(L_z/w_y)$, where κ_{yy} is the longitudinal thermal conductivity along the y axis (again taken to be equal to κ_{xx}).

Longitudinal thermal conductivity. As reported previously[4], we find that La_2CuO_4 has a nearly isotropic longitudinal thermal conductivity at low temperatures (Extended Data Fig. 2). Indeed, $\kappa_{xx}/\kappa_{zz}=\kappa_a/\kappa_c\approx0.8$ at $T=25$ K. At higher temperatures, thermally excited magnons contribute to heat transport in La_2CuO_4, but only along the plane, and κ_a grows to exceed κ_c (ref. [4]). As phonons dominate the heat transport at lower temperatures, the conductivity of phonons is nearly isotropic.

In Nd-LSCO, we also find that the phonon conductivity is nearly isotropic (deduced from the data in Extended Data Fig. 3). Once we remove the contribution of mobile charge carriers using the Wiedemann–Franz law, we have $\kappa_{xx}/\kappa_{zz}=\kappa_a/\kappa_c\approx1.2$ and 1.3 at $T=25$ K, for $p=0.21$ and $p=0.24$, respectively.

Note that the electrical conductivity, and therefore also the electronic thermal conductivity from charge carriers, is highly anisotropic, with $\sigma_{xx}/\sigma_{zz}=\rho_{zz}/\rho_{xx}\approx250$ in Nd-LSCO at $p=0.24$ (ref. [35]).

Anisotropy of the electronic Hall conductivity. The anisotropy of the electrical Hall conductivity in Nd-LSCO at $p=0.24$ is plotted as $L_0\,\sigma_{ny}$ versus T for $n=x$ and $n=z$ (Extended Data Fig. 4). We see that there is an anisotropy comparable to that found in the longitudinal conductivity, namely $\sigma_{xy}/\sigma_{zy}\sim250$. We expect that any excitation of electronic origin, arising from either charge or spin degrees of freedom, would yield a similarly strong anisotropy in both its longitudinal and transverse thermal conductivities. For that reason, we attribute the nearly isotropic thermal Hall conductivity found in La_2CuO_4 to phonons.

Wiedemann–Franz law for currents normal to the planes. In Nd-LSCO with $p=0.24$, the maximum contribution of charge carriers to $\kappa_{zy}(T)$ can be estimated using the Wiedemann–Franz law: $\kappa_{zy}/T\leq L_0\,\sigma_{zy}$, where $\sigma_{zy}\leq\rho_{zy}/(\rho_{zz}\rho_{yy})$. The data for ρ_{zz} and ρ_{zy} are displayed in Extended Data Fig. 5a,b, respectively. The ρ_{xx} data for the *a*-axis sample cut from the same crystal was reported in ref. [19]. The resulting curve for $L_0\,\sigma_{zy}$ (using $\rho_{yy}=\rho_{xx}$) is displayed in Extended Data Fig. 5c. As $\rho_{zz}/\rho_{xx}\sim250$ in Nd-LSCO at $p=0.24$, there is a correspondingly very small electrical Hall conductivity σ_{zy}. The maximum value of the electronic thermal Hall conductivity along the c axis is roughly $\kappa_{zy}/T\sim0.01$ mW K^{-2} m at $T=10$ K, a value 200 times smaller than the electronic thermal Hall conductivity measured in the plane (Fig. 1b). In Extended Data Fig. 5d, we see that this maximum electronic κ_{zy} is within the noise of the measured κ_{zy}. Any phonon contribution to κ_{zy} in Nd-LSCO at $p=0.24$ must therefore be smaller than $|\kappa_{zy}/T|\sim0.01$ mW K^{-2} m at $T=10$ K. This is smaller than the measured $|\kappa_{zy}/T|$ in Nd-LSCO at $p=0.21$ by a factor of ~100. In other words, the thermal Hall response of phonons in Nd-LSCO undergoes an increase of at least 100-fold immediately upon crossing below p^*.

Field dependence of the conductivities. We show how κ_{zz} and κ_{zy} vary with the strength of the applied field for three of our samples by plotting: κ_{zz} versus T at $H=0$, 10 and 15 T; and $\kappa_{zy}/(T\,H)$ versus T at $H=10$ and 15 T (Extended Data Fig. 6). In all cases, the field dependence of the thermal conductivity κ_{zz} is very small, and the thermal Hall conductivity κ_{zy} is essentially linear in H.

Background signal from the sample mount. As the sample is attached to a block of copper that serves as the heat sink in our experimental set-up (Extended Data Fig. 1), it might expected that a thermal Hall signal would come from copper. However, for all of the data reported here and those published in ref. [3], which were obtained using the same set-up, this background signal from copper was negligible, as demonstrated in three ways.

First, the fact that the Wiedemann–Franz law is satisfied for in-plane transport in Nd-LSCO at $p=0.24$ (ref. [3]) rules out any substantial contamination of the κ_{xy} data in that measurement.

Second, the fact that our *c*-axis data for Nd-LSCO and Eu-LSCO with $p = 0.24$ yield $|\kappa_{zy} / T| < 0.01$ mW K^{-2} m for all temperatures of up to at least 100 K (Fig. 1b,d) shows that the signal from copper is smaller than the noise in our measurement.

Third, we have carried out a test study whereby a cuprate sample was measured first in the usual way, using a copper block to which the sample was glued with silver paste, and then re-measured using a block of lithium fluoride (an insulator known to generate no thermal Hall signal) to which the sample was glued with GE varnish. All other aspects of the experiment were kept the same in the two measurements (contacts, wires, heater, thermometers, electronics). The thermal Hall signal obtained in the two separate ways was identical within error bars; that is, $\kappa_{xy}(T)$ was fully reproduced at all temperatures from 10 K to 100 K. These test data will be reported in a separate paper. The small level of contamination from the copper block is largely due to the mounting geometry such that the main (longitudinal) temperature gradient in the block is perpendicular to the main (longitudinal) temperature gradient in the sample (Extended Data Fig. 1).

Prior arguments against a phonon scenario. In ref. [3], it was considered unlikely that phonons could be responsible for the large negative thermal Hall signal κ_{xy} found in cuprates on the basis of two observations. First, the longitudinal phonon thermal conductivity κ_{xx} couples very weakly to the magnetic field. Specifically, κ_{xx} changes at most by 0.5% in fields of strength 15 T, and the maximal ratio $\kappa_{xy} / \kappa_{xx}$ is also about 0.5%. This is much smaller than in multiferroics[15], for example, in which phonons are thought to be responsible for the thermal Hall effect. This weak field dependence of κ_{xx} in cuprates is now one aspect of the phenomenology that needs to be understood.

The second observation is that the phonon part of the longitudinal thermal conductivity κ_{xx} increases upon crossing below $p^\star$ (ref. [3]), as opposed to the decrease expected if some new scattering mechanism of phonons (causing the chirality) appears in the pseudogap phase. An increase in κ_{xx} is natural in view of the large drop in the charge carrier density of Nd-LSCO below $p^\star$ (ref. [20]), which means that phonons become less scattered by electrons. Therefore, a putative extra scattering mechanism would have to overcompensate for the electron-phonon effect. At this stage, the quantitative aspects of these two scattering mechanisms are unknown. Also, it may be that a scattering mechanism is not really what confers chirality to phonons in the pseudogap phase. They may instead acquire a Berry curvature, for example, which may not have a large effect on κ_{xx}.

Crystal structure of Nd-LSCO. At low temperatures, the material $La_{1.6-x}Nd_{0.4}Sr_xCuO_4$ adopts the so-called LTT crystal structure for a range of Sr concentrations that extends down to at least $x = 0.10$ and up to at least $x = 0.25$ (ref. [36]). At $x = 0.20$ and $x = 0.25$, X-ray diffraction detects the structural transition into the LTT phase upon cooling at $T_{LTT} \sim 70$ K and 50 K (ref. [36]), respectively (Extended Data Fig. 7a). At temperatures above T_{LTT}, the structural phase is labelled LTO1 (low-temperature orthorhombic), with transitions at $T_{LTO1} \sim 250$ K and 150 K, for $x = 0.20$ and $x = 0.25$, respectively (ref. [36]).

Therefore, our two Nd-LSCO samples with nominal Sr concentrations $x = 0.21$ and $x = 0.25$, refined to $p = 0.21 \pm 0.003$ and $p = 0.24 \pm 0.005$, respectively, are expected to have the same crystal structure below 150 K. We have confirmed this by performing dilatometry measurements of the sample length L versus temperature in Nd-LSCO samples with $p = 0.21$ (the actual sample in which κ_{zy} was measured) and $p = 0.24$ (a sample cut immediately next to the sample in which κ_{zy} was measured). The data are shown in Extended Data Fig. 7b, plotted as dL / dT versus T. A clear anomaly is observed in both samples at the structural transition, with transition temperatures $T_{LTT} \sim 82 \pm 5$ K at $p = 0.21$ and $T_{LTT} \sim 45 \pm 10$ K at $p = 0.24$.

This confirms that there is no structural difference between our two Nd-LSCO samples with $p = 0.21$ and $p = 0.24$. Therefore, this rules out the possibility that the large phonon Hall effect observed at $p = 0.21$ but absent at $p = 0.24$ is due to structural domain boundaries that scatter phonons, as has been proposed for $SrTiO_3$ (ref. [16]), or to any other structural feature.

Data availability

All of the data that support the plots in this paper and other findings of this study are available from the corresponding author upon reasonable request. Source data are provided with this paper.

References

34. Grissonnanche, G. et al. Wiedemann–Franz law in the underdoped cuprate superconductor YBCO. *Phys. Rev. B* **93**, 064513 (2016).
35. Daou, R. et al. Linear temperature dependence of resistivity and change in the Fermi surface at the pseudogap critical point of a high-T_c superconductor. *Nat. Phys.* **5**, 31–34 (2009).
36. Axe, J. D. & Crawford, M. K. Structural instabilities in lanthanum cuprate superconductors. *J. Low Temp. Phys.* **95**, 271–284 (1994).

Acknowledgements

We thank L. Balents, K. Behnia, R. M. Fernandes, I. Garate, J. H. Han, C. Hess, S. A. Kivelson, P. A. Lee, A. H. MacDonald, J. E. Moore, B. J. Ramshaw, L. Savary, O. Sushkov, A.-M. S. Tremblay, R. Valenti and C. M. Varma for fruitful discussions. L.T. acknowledges support from the Canadian Institute for Advanced Research (CIFAR) as a Fellow, and funding from the Natural Sciences and Engineering Research Council of Canada (NSERC; PIN 123817), the Fonds de recherche du Québec – Nature et Technologies (FRQNT), the Canada Foundation for Innovation (CFI) and a Canada Research Chair. This research was undertaken thanks in part to funding from the Canada First Research Excellence Fund. Part of this work was funded by the EPiQS Initiative of the Gordon and Betty Moore Foundation (Grant GBMF5306 to L.T.). J.-S.Z. was supported by a US National Science Foundation grant (MRSEC DMR-1720595).

Author contributions

G.G., S.T., M.-E.B. and E.L. performed the thermal Hall conductivity measurements. A.G., A.A., F.L., M.D. and N.D.-L. prepared and characterized the samples. J.-S.Z. grew the Nd-LSCO single crystals. S.P., T.T. and H.T. grew the Eu-LSCO and La_2CuO_4 single crystals. G.G. and L.T. wrote the manuscript, in consultation with all of the authors. L.T. supervised the project.

Competing interests

The authors declare no competing interests.

Additional information

Extended data is available for this paper at https://doi.org/10.1038/s41567-020-0965-y.

Correspondence and requests for materials should be addressed to G.G. or L.T.

Peer review information *Nature Physics* thanks Liling Sun and the other, anonymous, reviewer(s) for their contribution to the peer review of this work.

Reprints and permissions information is available at www.nature.com/reprints.

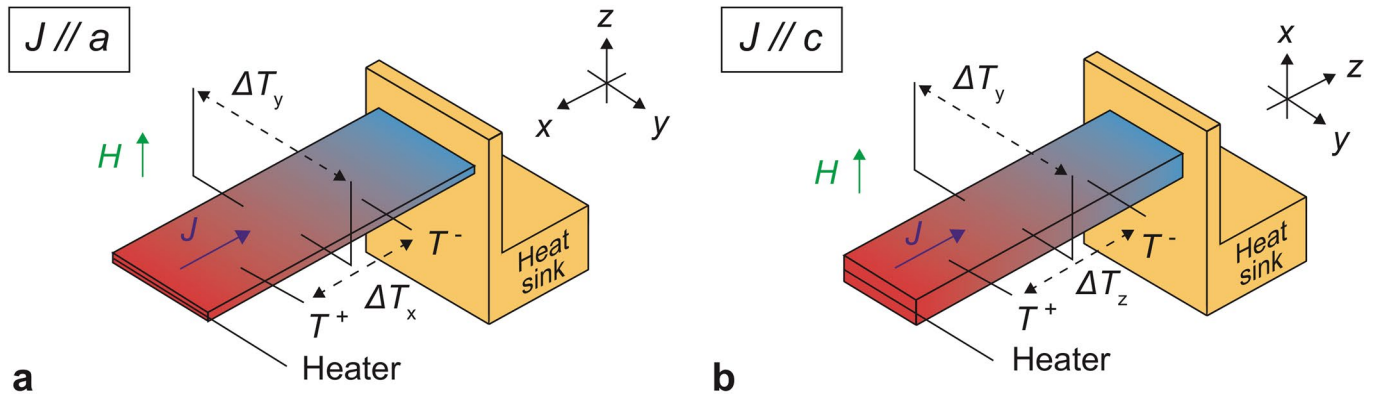

Extended Data Fig. 1 | Current and field orientation for κ_{xy} and κ_{zy} measurements. Sketch of the thermal Hall measurement setup for **a)** *J // a // -x* and **b)** *J // c // z*. The Cartesian coordinate system is defined in the same way for the two samples.

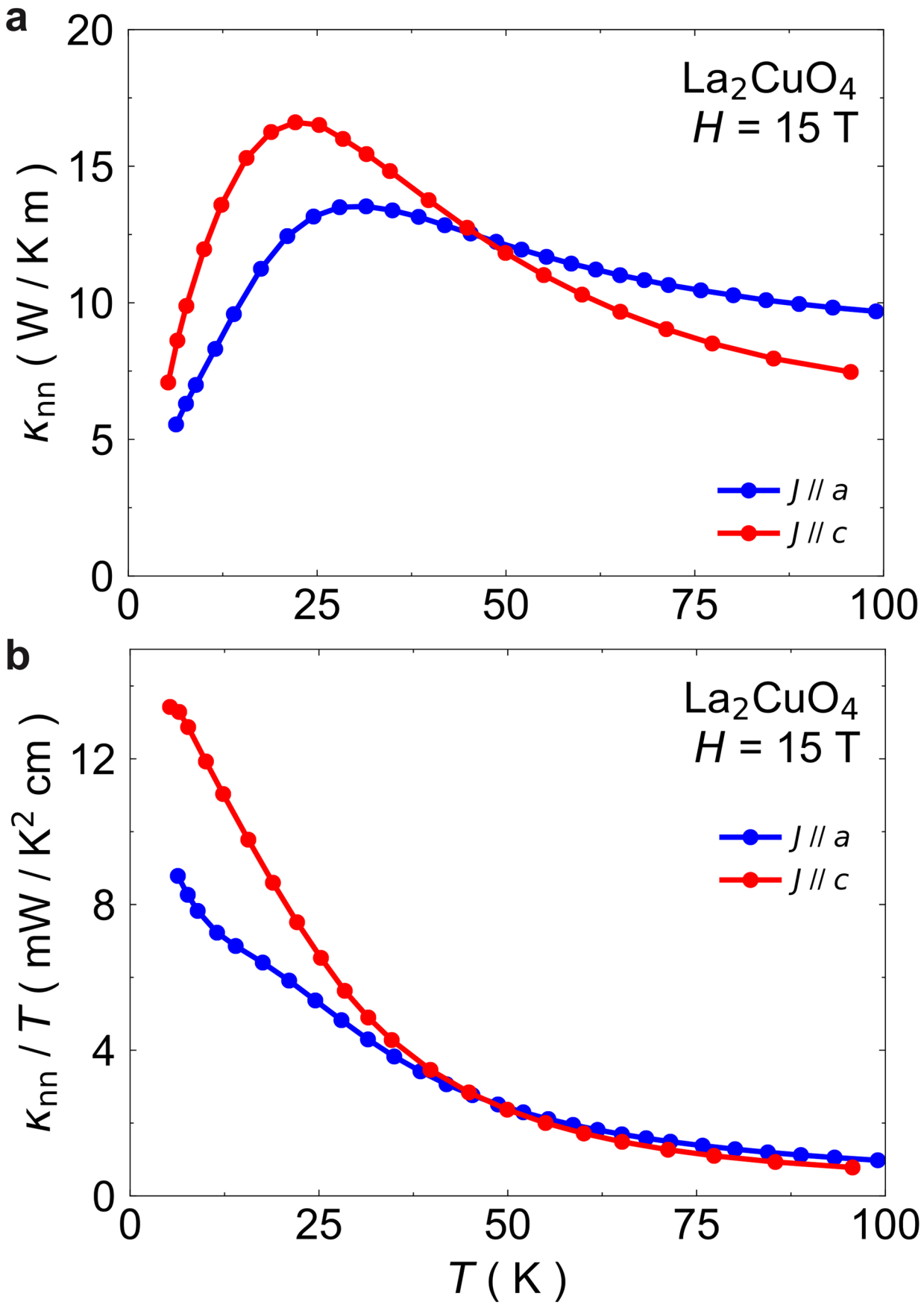

Extended Data Fig. 2 | Longitudinal thermal conductivities κ_{xx} and κ_{zz} in La_2CuO_4. Thermal conductivity versus temperature in a field of magnitude $H = 15$ T for La_2CuO_4 ($p = 0$), plotted as **a)** κ_{nn} vs T and **b)** κ_{nn} / T vs T, for heat current directions J // a ($n = x$; blue) and J // c ($n = z$; red). The longitudinal thermal conductivity of phonons at low temperature is nearly isotropic, with κ_{xx} / $\kappa_{zz} = \kappa_a$ / κ_c ~ 0.8 at $T = 25$ K.

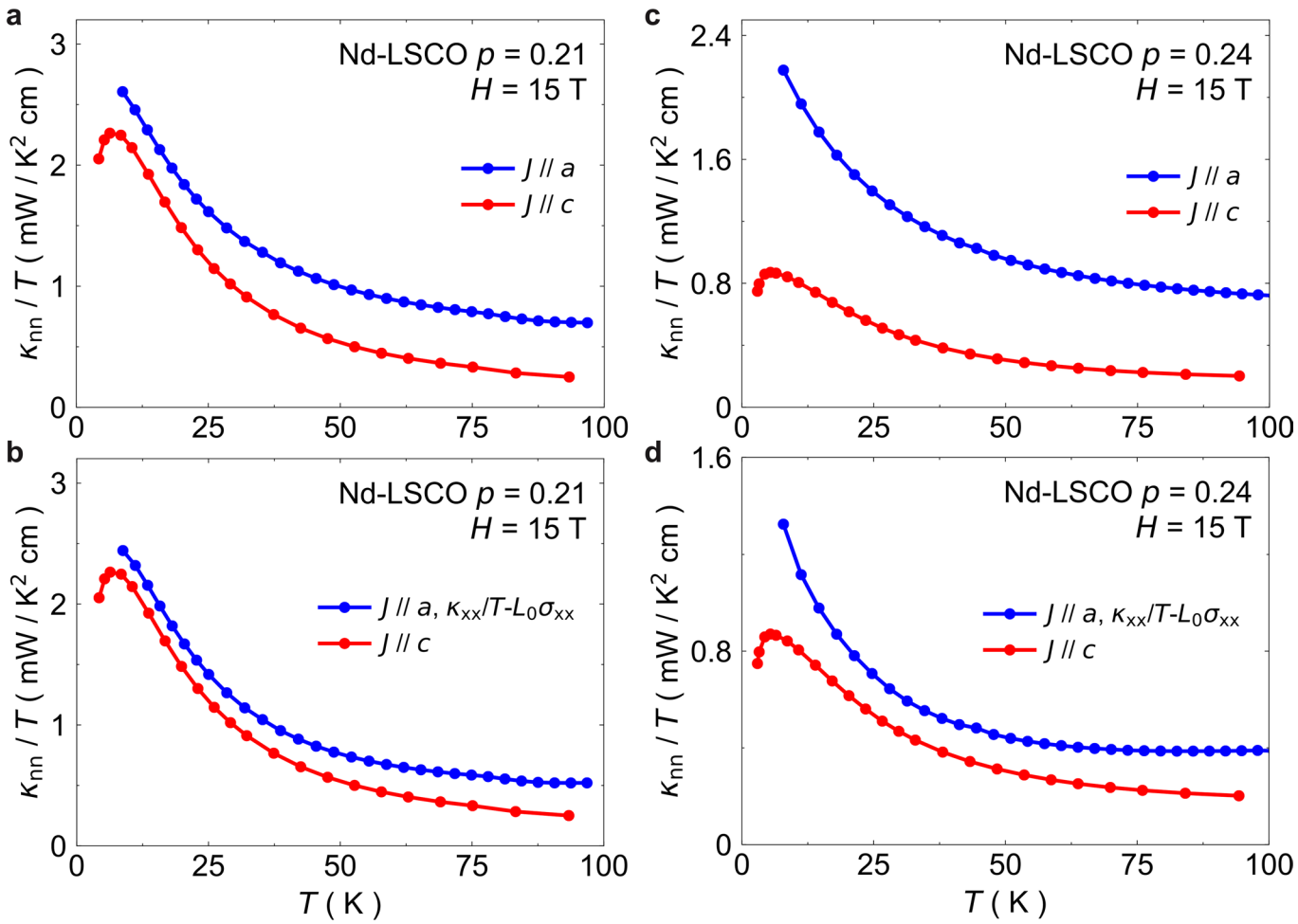

Extended Data Fig. 3 | Longitudinal thermal conductivities κ_{xx} and κ_{zz} in Nd-LSCO. Thermal conductivity κ_{nn} versus temperature in a field of magnitude $H = 15$ T, plotted as κ_{nn} / T vs T, for **a)** Nd-LSCO with $p = 0.21$ and **b)** Nd-LSCO with $p = 0.24$, for heat current directions $J // a$ ($n = x$; blue) and $J // c$ ($n = z$; red). In panels c) and d), the thermal conductivity of charge carriers is subtracted, using the Wiedemann-Franz law to estimate its magnitude (see ref. [3]). The longitudinal thermal conductivity of phonons at low temperature is nearly isotropic, with $\kappa_{xx} / \kappa_{zz} = \kappa_a / \kappa_c \sim 1.2$ and 1.3 at $T = 25$ K, for $p = 0.21$ and $p = 0.24$, respectively.

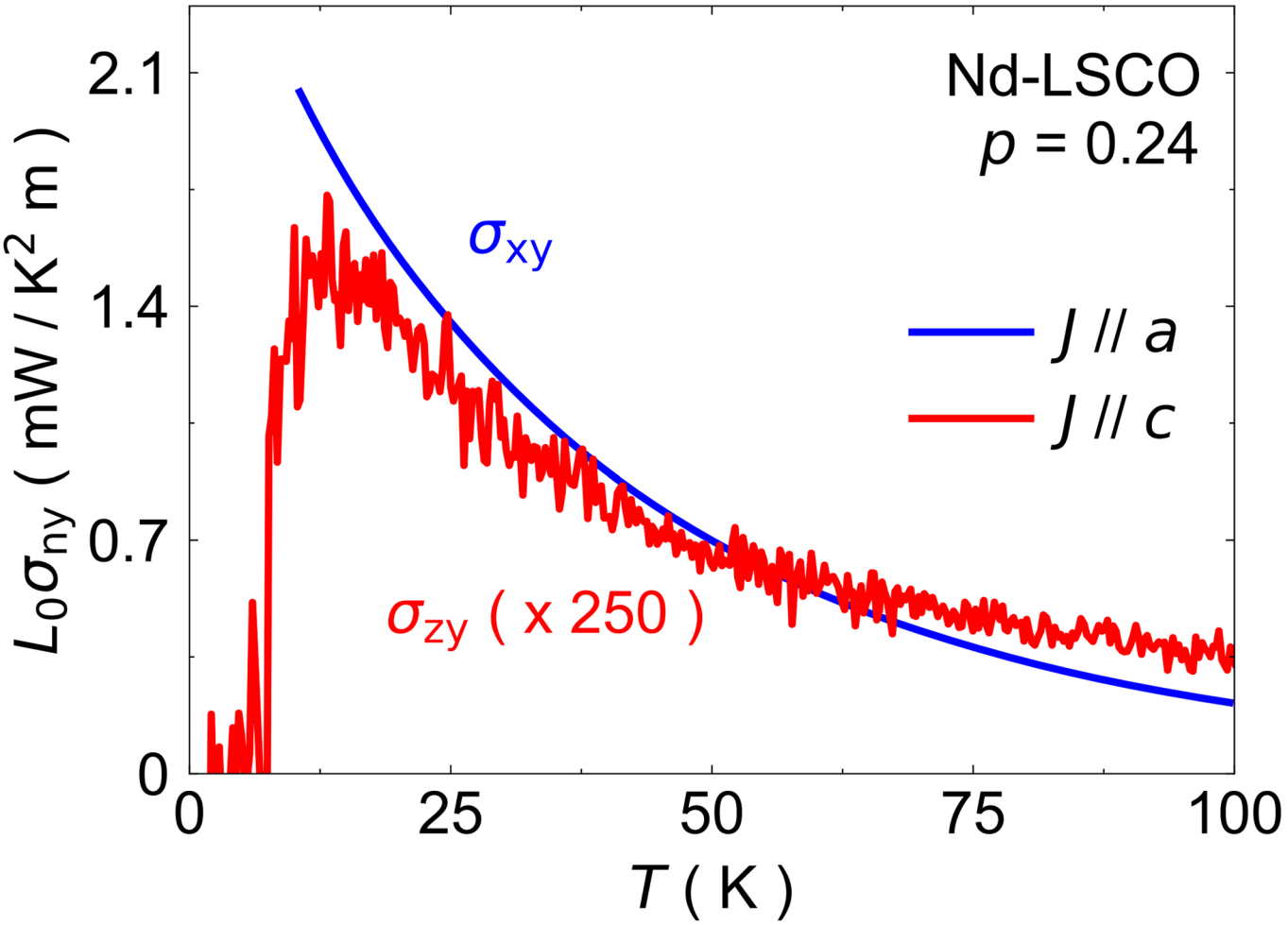

Extended Data Fig. 4 | Anisotropy of electrical Hall conductivity in Nd-LSCO. Electrical Hall conductivity σ_{ny} versus temperature in a field of magnitude $H = 15$ T, plotted as $L_0\,\sigma_{ny}$ vs T, for Nd-LSCO with $p = 0.24$, for heat current directions J // a ($n = x$; blue) and J // c ($n = z$; red). The data for σ_{zy} are multiplied by a factor 250. We use the approximate relation $\sigma_{zy} = \rho_{zy} / (\rho_{zz}\,\rho_{xx})$, with ρ_{zz} and ρ_{xx} data taken from ref. [35]. The σ_{xy} data are taken from ref. [3].

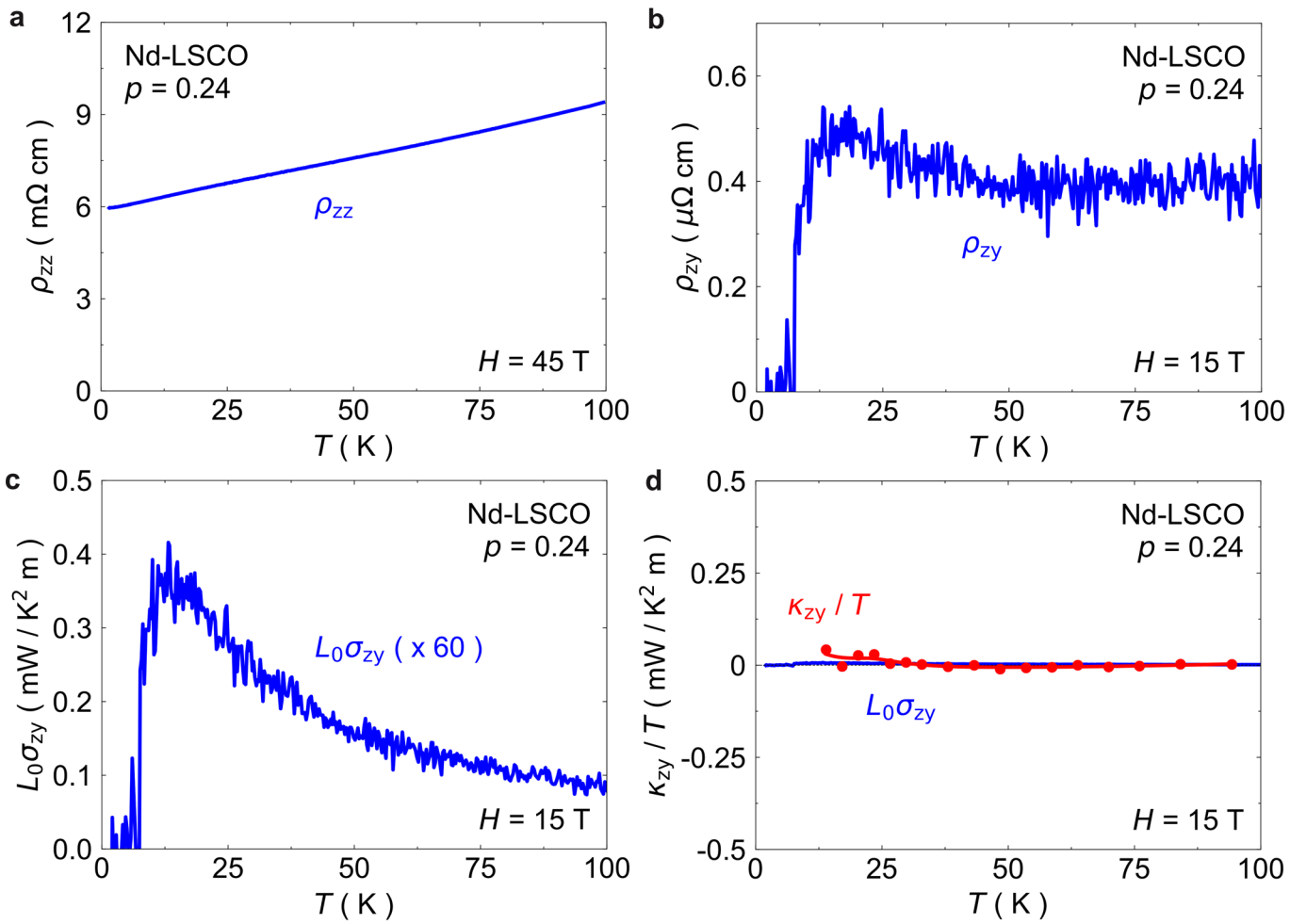

Extended Data Fig. 5 | Electronic thermal Hall conductivity in Nd-LSCO $p = 0.24$. Estimate of the maximal c-axis thermal Hall conductivity from charge carriers in our sample of Nd-LSCO with $p = 0.24$, obtained by applying the Wiedemann-Franz law to the measured electrical Hall conductivity σ_{zy}, namely $\kappa_{zy} / T \leq L_0 \sigma_{zy}$, where $\sigma_{zy} \leq \rho_{zy} / (\rho_{zz} \rho_{yy})$. **a)** Electrical resistivity for J // c, ρ_{zz} vs T (from ref. [35]); **b)** electrical Hall resistivity for J // c and H // a, ρ_{zy} vs T ; **c)** maximal electrical Hall conductivity for J // c and H // a, defined as $\sigma_{zy} = \rho_{zy} / (\rho_{zz} \rho_{xx})$ (with ρ_{xx} data from ref. [35]), plotted as $L_0 \sigma_{zy}$ (multiplied by 60) vs T ; **d)** comparison of the measured electrical (σ_{zy}) and thermal (κ_{zy}) Hall conductivities, plotted as $L_0 \sigma_{zy}$ (blue) and κ_{zy} / T (red; Fig. 1b) vs T.

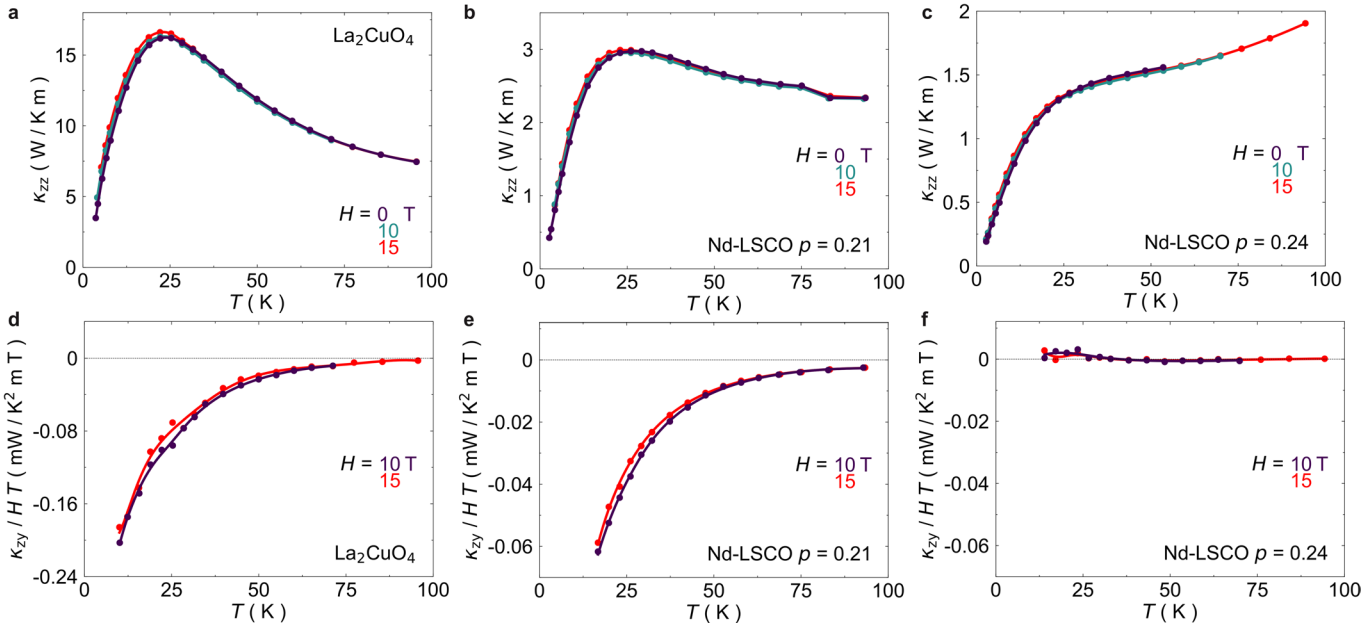

Extended Data Fig. 6 | Field dependence of κ_{zz} and κ_{zy} in La_2CuO_4 and Nd-LSCO. *Upper panels*: thermal conductivity κ_{zz} measured at $H = 0$ T (purple), 10 T (green) and 15 T (red), plotted as κ_{zz} / T vs T, for **a)** La_2CuO_4, **b)** Nd-LSCO with $p = 0.21$ and **c)** Nd-LSCO with $p = 0.24$. *Lower panels*: thermal Hall conductivity κ_{zy} measured at $H = 10$ T (purple) and 15 T (red), plotted as $\kappa_{zy} / (T H)$ vs T, for **d)** La_2CuO_4, **e)** Nd-LSCO with $p = 0.21$ and **f)** Nd-LSCO with $p = 0.24$. We see that κ_{zy} is approximately linear in H.

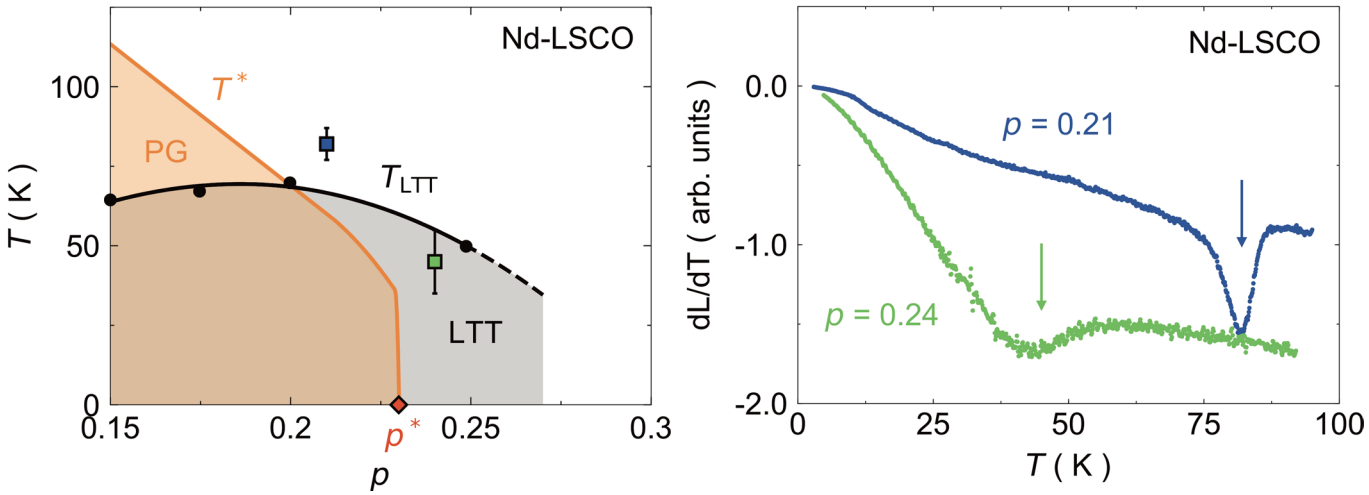

Extended Data Fig. 7 | Structural transition in Nd-LSCO. a) Structural phase diagram of Nd-LSCO as a function of doping. The black dots and black line mark the structural transition from the LTO1 phase to the LTT phase at low temperature, at T_{LTT}, as measured by x-ray diffraction[36]. The squares mark T_{LTT} in our samples with $p = 0.21$ (blue) and $p = 0.24$ (green), as detected by dilatometry measurements (see panel b). **b)** Change in sample length L as a function of temperature, plotted as its derivative dL / dT vs T, measured in our c-axis sample of Nd-LSCO with $p = 0.21$ (blue) and in a sample of Nd-LSCO cut from the same large single crystal as, and next to, our c-axis sample of Nd-LSCO with $p = 0.24$ (green). The dip in the curves marks the structural phase transition from the LTO1 phase above to the LTT phase below the transition temperature T_{LTT}, where $T_{LTT} = 82 \pm 5$ K at $p = 0.21$ and $T_{LTT} = 45 \pm 10$ K at $p = 0.24$. The error bars on the two values of T_{LTT} correspond to the full width of each corresponding dip. These data confirm that our two Nd-LSCO samples, with $p = 0.21$ and $p = 0.24$, have the same crystal structure. This shows that all the differences observed in their properties, in particular the dramatic difference in their thermal Hall conductivity κ_{xy} (Fig. 1), are not due to a difference in structural properties. Instead, these differences are linked with the onset of the pseudogap phase at $p^* = 0.23$.